B-spline neural network based single-carrier frequency domain equalisation for Hammerstein channels

B-Spline Neural Network Based Single-Carrier Frequency Domain Equalisation for Hammerstein Channels

Xia Hong, Sheng Chen and Chris J. Harris

Abstract— **A practical single-carrier (SC) block transmission with frequency domain equalisation (FDE) system can generally be modelled by the Hammerstein system that includes the nonlinear distortion effects of the high power amplifier (HPA) at transmitter. For such Hammerstein channels, the standard SC-FDE scheme no longer works. We propose a novel B-spline neural network based nonlinear SC-FDE scheme for Hammerstein channels. In particular, we model the nonlinear HPA, which represents the complex-valued static nonlinearity of the Hammerstein channel, by two real-valued B-spline neural networks, one for modelling the nonlinear amplitude response of the HPA and the other for the nonlinear phase response of the HPA. We then develop an efficient alternating least squares algorithm for estimating the parameters of the Hammerstein channel, including the channel impulse response coefficients and the parameters of the two B-spline models. Moreover, we also use another real-valued B-spline neural network to model the inversion of the HPA's nonlinear amplitude response, and the parameters of this inverting B-spline model can be estimated using the standard least squares algorithm based on the pseudo training data obtained as a byproduct of the Hammerstein channel identification. Equalisation of the SC Hammerstein channel can then be accomplished by the usual one-tap linear equalisation in frequency domain as well as the inverse B-spline neural network model obtained in time domain. The effectiveness of our nonlinear SC-FDE scheme for Hammerstein channels is demonstrated in a simulation study.**

I. Introduction

The fourth generation (4G) and beyond 4G (B4G) mobile communication systems support high-speed broadband applications with data rates in tens of Mbps or higher over the wireless channel of typical delay spread in microseconds. The intersymbol interference (ISI) of such wireless channels spans over tens or even hundreds of symbols, which causes the nightmare senario for time-domain (TD) equalisation, requiring an impractically long equaliser with excessively slow convergence and therefore resulting in poor performance. Orthogonal frequency-division multiplexing (OFDM) [1], [2] offers a low-complexity high-performance solution for mitigating long ISI. Owing to its virtues of resilience to frequency selective fading channels, OFDM has found its way into numerous recent wireless network standards. However, an OFDM signal is notoriously known to have high peak-to-average power ratio (PAPR), which requires the high power amplifier (HPA) at the transmitter to have an extremely long linear dynamic range. This requirement may not be met by practical HPAs which exhibits nonlinear saturation characteristics [3]–[7]. An alternative solution for long ISI mitigation is to adopt single-carrier (SC) block transmission with frequency-domain equalisation (FDE) [8], [9]. Although the total complexity of a SC-FDE based transceiver is the same as that of an OFDM based transceiver, the SC-FDE transmitter does not require the fast Fourier transform (FFT) operation, and therefore it is better suited for uplink implementation. The long term evolution advanced (LTE-A) has specified the standard for the uplink of the 4G and B4G systems based on the SC-FDE solution [10].

In order to enhance the achievable bandwidth efficiency, SC based broadband systems typically adopt high-order quadrature amplitude modulation (QAM) signalling [11]. The higher the order of QAM signalling, the better the bandwidth efficiency but also the higher the PAPR of the resulting transmit signal. This may drive the HPA at the transmitter into the nonlinear saturation region, which will significantly degrade the system's achievable bit error rate (BER) performance. Therefore, it is important to be able to effectively compensate the nonlinear distortions of the HPA in the design of a SC based high-rate wireless system. An effective approach to compensate the nonlinear distortions of HPA is to implement a digital predistorter at the transmitter, which is capable of achieving excellent performance, and various predistorter techniques have been developed [12]–[18]. Implementing the predistorter is attractive for the downlink, where the base station (BS) transmitter has the sufficient hardware and software capacities to accommodate the hardware and computational requirements for implementing digital predistorter. In the uplink, however, implementing predistorter at transmitter is much more difficult, as it is extremely challenging for a pocket-size handset to absorb the additional hardware and computational complexity. Therefore, the predistorter option is not viable for the SC-FDE based uplink. Alternatively, the nonlinear distortions of the transmitter HPA can be dealt with at the BS receiver, which has sufficient hardware and software resources. With the nonlinear HPA at transmitter, the channel is a complex-valued (CV) Hammerstein system and, moreover, the received signal is further impaired by the channel additive white Gaussian noise (AWGN). Therefore, nonlinear equalisation of the SC based Hammerstein channel is a challenging task.

In this contribution, we propose an efficient nonlinear SC-FDE scheme for Hammerstein channels based on the B-spline neural network. In our previous works [18], [19], the B-spline neural network has been demonstrated to be very effective in identification and inversion of CV Wiener

X. Hong is with School of Systems Engineering, University of Reading, Reading RG6 6AY, U.K. (E-mail: x.hong@reading.ac.uk).

S. Chen and C.J. Harris are with Electronics and Computer Science, University of Southampton, Southampton SO17 1BJ, UK (E-mails: sqc@ecs.soton.ac.uk, cjh@ecs.soton.ac.uk). S. Chen is also with King Abdulaziz University, Jeddah 21589, Saudi Arabia.

systems. We adopt two real-valued (RV) B-spline neural networks to model the amplitude response and the phase response of the CV static nonlinearity of the Hammerstein channel, and we develop a highly efficient alternating least squares (ALS) identification algorithm for estimating the channel impulse response (CIR) coefficients as well as the parameters of the two RV B-spline neural networks that model the HPA's CV static nonlinearity. As linear equalisation is naturally accomplished in SC-FDE based systems by a one-tap equalisation in frequency domain (FD), nonlinear SC-FDE of the Hammerstein channel additionally involves the inversion of the estimated B-spline neural network that models the HPA's nonlinear amplitude response in TD, as the compensation of the HPA's nonlinear phase response is straightforward using the estimated phase response. The previous work [18] considers the inversion of a RV B-spline model as the root finding problem, and develop an iterative root finding procedure based on the Gauss-Newton algorithm for inverting the estimated amplitude response. This approach requires to carry out the iterative root finding procedure for detecting every data symbol. We propose a much faster and more efficient alternative for inverting the HPA's nonlinear amplitude response. Specifically, we use another RV B-spline neural network to model the inversion of the HPA's nonlinear amplitude response. Although the HPA's output at the transmitter is unobservable at the receiver for identifying this inverse model, the pseudo training data obtained as a natural byproduct of the Hammerstein channel identification can be used to estimate the parameters of the inverting B-spline model using the standard least squares (LS) algorithm. We demonstrate the effectiveness of our proposed B-spline neural network based SC-FDE scheme for Hammerstein channels in an extensive simulation study.

Throughout this contribution, a CV number $x \in \mathbb{C}$ is represented either by the rectangular form $x = x_R + \mathrm{j} \cdot x_I$, where $\mathrm{j} = \sqrt{-1}$, while $x_R = \Re[x]$ and $x_I = \Im[x]$ denote the real and imaginary parts of x, or alternatively by the polar form $x = |x| \cdot e^{\mathrm{j}\angle^x}$ with $|x|$ denoting the amplitude of x and $\angle^x$ its phase. The vector or matrix transpose and conjugate transpose operators are denoted by $(\ )^{\mathrm{T}}$ and $(\ )^{\mathrm{H}}$, respectively, while $(\ )^{-1}$ stands for the inverse operation and the expectation operator is denoted by $\mathrm{E}\{\ \}$. Furthermore, $\boldsymbol{I}$ denotes the identity matrix with an appropriate dimension, and $\mathrm{diag}\{x_0, x_1, \cdots, x_{n-1}\}$ is the diagonal matrix with $x_0, x_1, \cdots, x_{n-1}$ as its diagonal elements.

II. Hammerstein Channel Model for SC-FDE

We consider the M-QAM signalling. Each transmit block or frame consists of N QAM data symbols expressed as

$$\boldsymbol{x}[s] = \big[x_0[s]\ x_1[s] \cdots x_{N-1}[s]\big]^{\mathrm{T}}, \tag{1}$$

where $[s]$ denotes the block index, and $x_k[s]$, $0 \le k \le N-1$, take the values from the M-QAM symbol set

$$\mathbb{X} = \{d(2l - \sqrt{M} - 1) + \mathrm{j} \cdot d(2q - \sqrt{M} - 1), 1 \le l, q \le \sqrt{M}\}, \tag{2}$$

where $2d$ is the minimum distance between symbol points. For notational simplification, we will drop the block index $[s]$ in the sequel. Adding the cyclic prefix (CP) of length N_{cp} to $\boldsymbol{x}$ yields

$$\bar{\boldsymbol{x}} = \big[x_{-N_{\mathrm{cp}}}\ x_{-N_{\mathrm{cp}}+1} \cdots x_{-1} \mid \boldsymbol{x}^{\mathrm{T}}\big]^{\mathrm{T}}, \tag{3}$$

in which $x_{-k} = x_{N-k}$ for $1 \le k \le N_{\mathrm{cp}}$. The signal block $\bar{\boldsymbol{x}}$ is amplified by the HPA to yield the actually transmitted signal vector

$$\begin{aligned} \bar{\boldsymbol{w}} &= \big[w_{-N_{\mathrm{cp}}}\ w_{-N_{\mathrm{cp}}+1} \cdots w_{-1} \mid w_0\ w_1 \cdots w_{N-1}\big]^{\mathrm{T}} \\ &= \big[w_{-N_{\mathrm{cp}}}\ w_{-N_{\mathrm{cp}}+1} \cdots w_{-1} \mid \boldsymbol{w}^{\mathrm{T}}\big]^{\mathrm{T}} \end{aligned} \tag{4}$$

where

$$w_k = \Psi(x_k),\ -N_{\mathrm{cp}} \le k \le N-1, \tag{5}$$

in which $\Psi(\ )$ represents the CV static nonlinearity of the transmitter HPA, and $w_{-k} = w_{N-k}$ for $1 \le k \le N_{\mathrm{cp}}$. We consider the solid state power amplifier [6], [7], whose nonlinearity $\Psi(\ )$ is constituted by the HPA's amplitude response $A(r)$ and phase response $\Upsilon(r)$ given by

$$A(r) = \frac{g_a r}{\left(1 + \left(\frac{g_a r}{A_{\mathrm{sat}}}\right)^{2\beta_a}\right)^{\frac{1}{2\beta_a}}}, \tag{6}$$

$$\Upsilon(r) = \frac{\alpha_\phi r^{q_1}}{1 + \left(\frac{r}{\beta_\phi}\right)^{q_2}}, \tag{7}$$

where r denotes the amplitude of the input to the HPA, g_a is the small gain signal, β_a is the smoothness factor and A_{sat} is the saturation level, while the parameters of the phase response, α_ϕ. β_ϕ, q_1 and q_2, are adjusted to match the specific amplifier's characteristics. The NEC GaAs power amplifier used in the standardization [6], [7] has the the parameter set

$$\begin{aligned} &g_a = 19,\ \beta_a = 0.81,\ A_{\mathrm{sat}} = 1.4; \\ &\alpha_\phi = -48000,\ \beta_\phi = 0.123,\ q_1 = 3.8,\ q_2 = 3.7. \end{aligned} \tag{8}$$

Hence, given the input $x_k = |x_k| \cdot e^{\mathrm{j} \cdot \angle^{x_k}}$, the output of the HPA can be expressed as

$$w_k = A(|x_k|) \cdot e^{\mathrm{j} \cdot \left(\angle^{x_k} + \Upsilon(|x_k|)\right)}. \tag{9}$$

The operating status of the HPA may be specified by the output back-off (OBO), which is defined as the ratio of the maximum output power $P_{\max}$ of the HPA to the average output power P_{aop} of the HPA output signal, given by

$$\mathrm{OBO} = 10 \cdot \log_{10} \frac{P_{\max}}{P_{\mathrm{aop}}}. \tag{10}$$

The smaller OBO is, the more the HPA is operating into the nonlinear saturation region.

The amplified signal $\bar{\boldsymbol{w}}$ is transmitted through the channel whose CIR coefficient vector is expressed by

$$\boldsymbol{h} = \big[h_0\ h_1 \cdots h_{L_{\mathrm{cir}}}\big]^{\mathrm{T}}. \tag{11}$$

The CIR length satisfies $L_{\mathrm{cir}} \le N_{\mathrm{cp}}$. It is assumed that $h_0 = 1$ because if this is not the case, h_0 can always be absorbed

into the CV static nonlinearity $\Psi(\ )$, and the channel impulse response coefficients are re-scaled as h_i/h_0 for $0 \le i \le L_{\rm cir}$. At the receiver, after the CP removal, the channel-impaired received signals y_k are given by

$$y_k = \sum_{i=0}^{L_{\rm cir}} h_i w_{k-i} + e_k,\ 0 \le k \le N-1, \tag{12}$$

in which $w_{k-i} = w_{N+k-i}$ for $k < i$, where $e_k = e_{k_R} + \mathrm{j}\cdot e_{k_I}$ is the channel AWGN with $E\{e_{k_R}^2\} = E\{e_{k_I}^2\} = \sigma_e^2$. Because $N_{\rm cp} \ge L_{\rm cir}$, the CP removal at the receiver automatically cancels the inter block interference and transfers the linear convolution channel into the circular one. Passing $\boldsymbol{y} = \begin{bmatrix} y_0\ y_1 \cdots y_{N-1} \end{bmatrix}^{\rm T}$ through the N-point FFT processor yields the FD received signal vector

$$\boldsymbol{Y} = \begin{bmatrix} Y_0\ Y_1 \cdots Y_{N-1} \end{bmatrix}^{\rm T} = \boldsymbol{F}\boldsymbol{y}, \tag{13}$$

where

$$\boldsymbol{F} = \frac{1}{\sqrt{N}} \begin{bmatrix} 1 & 1 & \cdots & 1 \\ 1 & e^{-\mathrm{j}2\pi/N} & \cdots & e^{-\mathrm{j}2\pi(N-1)/N} \\ \vdots & \vdots & \vdots & \vdots \\ 1 & e^{-\mathrm{j}2\pi(N-1)/N} & \cdots & e^{-\mathrm{j}2\pi(N-1)(N-1)/N} \end{bmatrix}, \tag{14}$$

is the FFT matrix which has the orthogonal property of $\boldsymbol{F}^{\rm H}\boldsymbol{F} = \boldsymbol{F}\boldsymbol{F}^{\rm H} = \boldsymbol{I}$. The elements of $\boldsymbol{Y}$ are given by

$$Y_n = H_n W_n + \Xi_n,\ 0 \le n \le N-1, \tag{15}$$

where $\Xi_n = \Xi_{n_R} + \mathrm{j}\cdot\Xi_{n_I}$ is the FD channel AWGN with $E\{\Xi_{n_R}^2\} = E\{\Xi_{n_I}^2\} = \sigma_e^2$, and the frequency domain channel transfer function coefficients (FDCTFCs) H_n for $0 \le n \le N-1$ are given by the N-point FFT of $\boldsymbol{h}$

$$\begin{bmatrix} H_0\ H_1 \cdots H_{N-1} \end{bmatrix}^{\rm T} = \boldsymbol{F}\boldsymbol{h}, \tag{16}$$

while

$$\boldsymbol{W} = \begin{bmatrix} W_0\ W_1 \cdots W_{N-1} \end{bmatrix}^{\rm T} = \boldsymbol{F}\boldsymbol{w} \tag{17}$$

is the N-point FFT of $\boldsymbol{w}$. Note that $\boldsymbol{w}$ is unobservable and, therefore, neither $\boldsymbol{w}$ nor $\boldsymbol{W}$ is available at the receiver. If we denote $\boldsymbol{\Xi} = \begin{bmatrix} \Xi_0\ \Xi_1 \cdots \Xi_{N-1} \end{bmatrix}^{\rm T}$, the FD received signal (15) can be expressed concisely as

$$\begin{aligned} \boldsymbol{Y} &= \mathrm{diag}\{H_0, H_1, \cdots, H_{N-1}\}\boldsymbol{W} + \boldsymbol{\Xi} \\ &= \mathrm{diag}\{H_0, H_1, \cdots, H_{N-1}\}\boldsymbol{F}\boldsymbol{w} + \boldsymbol{\Xi}. \end{aligned} \tag{18}$$

Given the FDCTFCs H_n for $0 \le n \le N-1$, the FD one-tap zero-forcing equalisation is given by

$$\widetilde{W}_n = \frac{Y_n}{H_n},\ 0 \le n \le N-1. \tag{19}$$

Performing the N-point inverse FFT (IFFT) on $\widetilde{\boldsymbol{W}} = \begin{bmatrix} \widetilde{W}_0\ \widetilde{W}_1 \cdots \widetilde{W}_{N-1} \end{bmatrix}^{\rm T}$ yields

$$\widetilde{\boldsymbol{w}} = \begin{bmatrix} \widetilde{w}_0\ \widetilde{w}_1 \cdots \widetilde{w}_{N-1} \end{bmatrix}^{\rm T} = \boldsymbol{F}^{\rm H}\widetilde{\boldsymbol{W}} = \boldsymbol{\Psi}(\boldsymbol{x}) + \boldsymbol{F}^{\rm H}\widetilde{\boldsymbol{\Xi}}, \tag{20}$$

where $\widetilde{\boldsymbol{\Xi}} = \mathrm{diag}\{H_0^{-1}, H_1^{-1}, \cdots, H_{N-1}^{-1}\}\boldsymbol{\Xi}$, and

$$\begin{aligned} \boldsymbol{\Psi}(\boldsymbol{x}) &= \begin{bmatrix} \Psi(x_0)\ \Psi(x_1) \cdots \Psi(x_{N-1}) \end{bmatrix}^{\rm T} \\ &= \begin{bmatrix} w_0\ w_1 \cdots w_{N-1} \end{bmatrix}^{\rm T}. \end{aligned} \tag{21}$$

If the HPA $\Psi(\ )$ at the transmitter were linear, $\widetilde{w}_k$ would be an estimate of the transmitted data symbol x_k. But $\Psi(\ )$ is nonlinear, and the linear equalisation (19) alone is no longer sufficient for estimating $\boldsymbol{x}$. If the nonlinearity $\Psi(\ )$ is known and it is invertible, then the effects of $\Psi(\ )$ can be compensated by inverting it. Specifically, an estimate of the transmitted data vector $\boldsymbol{x}$ is given by

$$\widehat{\boldsymbol{x}} = \boldsymbol{\Psi}^{-1}(\widetilde{\boldsymbol{w}}) = \begin{bmatrix} \Psi^{-1}(\widetilde{w}_0)\ \Psi^{-1}(\widetilde{w}_1) \cdots \Psi^{-1}(\widetilde{w}_{N-1}) \end{bmatrix}^{\rm T}. \tag{22}$$

III. Nonlinear SC-FDE of Hammerstein System

A. Identification of the Hammerstein channel

Given the input x_k to the HPA, we model the HPA's nonlinear amplitude response and phase response by the two RV univariate B-spline neural networks

$$\widehat{A}(|x_k|) = \sum_{l=1}^{N_b} B_l^{(P_o)}(|x_k|)\omega_l, \tag{23}$$

$$\widehat{\Upsilon}(|x_k|) = \sum_{l=1}^{N_b} B_l^{(P_o)}(|x_k|)\theta_l, \tag{24}$$

where N_b is the number of B-spline basis functions, $(P_o - 1)$ is the order of the piecewise polynomial and the B-spline basis functions $B_l^{(P_o)}(r)$ are calculated based on the De Boor algorithm given in Appendix A, while $\boldsymbol{\omega} = \begin{bmatrix} \omega_1\ \omega_2 \cdots \omega_{N_b} \end{bmatrix}^{\rm T}$ and $\boldsymbol{\theta} = \begin{bmatrix} \theta_1\ \theta_2 \cdots \theta_{N_b} \end{bmatrix}^{\rm T}$ are the parameter vectors of the two RV B-spline models to be determined. The predicted HPA's output can then be expressed as

$$\widehat{w}_k = \widehat{A}(|x_k|) \cdot e^{\mathrm{j}\cdot\left(\angle x_k + \widehat{\Upsilon}(|x_k|)\right)}. \tag{25}$$

The identification task is to jointly estimate the CIR vector $\boldsymbol{h}$ and the parameter vectors $\{\boldsymbol{\omega}, \boldsymbol{\theta}\}$ based on a block of training data $\{x_k, y_k\}_{k=0}^{N-1}$ by minimising the cost function

$$J_1(\boldsymbol{h}, \boldsymbol{\omega}, \boldsymbol{\theta}) = \frac{1}{N}\sum_{k=0}^{N-1} \left|\widehat{e}_k\right|^2 = \frac{1}{N}\sum_{k=0}^{N-1} \left|y_k - \widehat{y}_k\right|^2 \tag{26}$$

subject to the constraint $h_0 = 1$, in which $\widehat{y}_k$ is given by

$$\widehat{y}_k = \sum_{i=0}^{L_{\rm cir}} h_i \widehat{w}_{k-i} = \sum_{i=0}^{L_{\rm cir}} h_i \widehat{A}(|x_{k-i}|) \cdot e^{\mathrm{j}\cdot\left(\angle x_{k-i} + \widehat{\Upsilon}(|x_{k-i}|)\right)}, \tag{27}$$

where $x_{k-i} = x_{N+k-i}$ and $\widehat{w}_{k-i} = \widehat{w}_{N+k-i}$ if $k < i$. By denoting $\widehat{\boldsymbol{e}} = \begin{bmatrix} \widehat{e}_0\ \widehat{e}_1 \cdots \widehat{e}_{N-1} \end{bmatrix}^{\rm T}$ and $\boldsymbol{y} = \begin{bmatrix} y_0\ y_1 \cdots y_{N-1} \end{bmatrix}^{\rm T}$ over the training data set, the system can be expressed as

$$\boldsymbol{y} = \boldsymbol{P}\boldsymbol{h} + \widehat{\boldsymbol{e}}, \tag{28}$$

where the regression matrix $\boldsymbol{P} \in \mathbb{C}^{N \times (L_{\rm cir}+1)}$ is given by

$$\boldsymbol{P} = \begin{bmatrix} \widehat{w}_0 & \widehat{w}_{-1} & \cdots & \widehat{w}_{-L_{\rm cir}} \\ \vdots & \vdots & \vdots & \vdots \\ \widehat{w}_k & \widehat{w}_{k-1} & \cdots & \widehat{w}_{k-L_{\rm cir}} \\ \vdots & \vdots & \vdots & \vdots \\ \widehat{w}_{N-1} & \widehat{w}_{N-2} & \cdots & \widehat{w}_{N-1-L_{\rm cir}} \end{bmatrix}. \tag{29}$$

Therefore, given $\boldsymbol{\omega}$ and $\boldsymbol{\theta}$, $\widehat{w}_k$ for $-L_{\rm cir} \le k \le N-1$ are fixed, and we have the LS estimate of $\boldsymbol{h}$ readily given by

$$\widehat{\boldsymbol{h}} = \left(\boldsymbol{P}^{\rm H}\boldsymbol{P}\right)^{-1}\boldsymbol{P}^{\rm H}\boldsymbol{y}. \tag{30}$$

When $\boldsymbol{h}$ is fixed, the FDE (19) can be carried out and the corresponding TD signal $\widetilde{w}_k$ of (20) can be calculated based on which we estimate $\{\boldsymbol{\omega}, \boldsymbol{\theta}\}$ by solving the optimisation

$$\min_{\boldsymbol{\omega},\boldsymbol{\theta}} J_2(\boldsymbol{\omega},\boldsymbol{\theta}) = \min_{\boldsymbol{\omega},\boldsymbol{\theta}} \frac{1}{N}\sum_{k=0}^{N-1}\left|\widetilde{w}_k - \widehat{A}(|x_k|)\cdot e^{{\rm j}\left(\angle^{x_k}+\widehat{\Upsilon}(|x_k|)\right)}\right|^2. \tag{31}$$

However, this is a complex nonlinear optimisation problem, requiring iterative calculation. To get around this difficulty, we relax our optimisation task into the two simultaneous objectives for $\boldsymbol{\omega}$ and $\boldsymbol{\theta}$, respectively,

$$\min_{\boldsymbol{\omega}} J_3(\boldsymbol{\omega}) = \min_{\boldsymbol{\omega}} \frac{1}{N}\sum_{k=0}^{N-1}\left(\left|\widetilde{w}_k\right| - \sum_{l=1}^{N_b} B_l^{(P_o)}(|x_k|)\omega_l\right)^2, \tag{32}$$

$$\min_{\boldsymbol{\theta}} J_4(\boldsymbol{\theta}) = \min_{\boldsymbol{\theta}} \frac{1}{N}\sum_{k=0}^{N-1}\left(\gamma_k - \sum_{l=1}^{N_b} B_l^{(P_o)}(|x_k|)\theta_l\right)^2, \tag{33}$$

where $-\pi < \gamma_k < \pi$ is the principle value of $\arctan\dfrac{\widetilde{w}_k}{x_k}$. The LS estimates of $\boldsymbol{\omega}$ and $\boldsymbol{\theta}$ are given respectively by

$$\widehat{\boldsymbol{\omega}} = \left(\mathbf{B}^{\rm T}\mathbf{B}\right)^{-1}\mathbf{B}^{\rm T}\left|\widetilde{\boldsymbol{w}}\right|, \tag{34}$$

$$\widehat{\boldsymbol{\theta}} = \left(\mathbf{B}^{\rm T}\mathbf{B}\right)^{-1}\mathbf{B}^{\rm T}\boldsymbol{\gamma}, \tag{35}$$

where $\left|\widetilde{\boldsymbol{w}}\right| = \left[\left|\widetilde{w}_0\right| \ \left|\widetilde{w}_1\right| \cdots \left|\widetilde{w}_{N-1}\right|\right]^{\rm T}$, $\boldsymbol{\gamma} = \left[\gamma_0 \ \gamma_1 \cdots \gamma_{N-1}\right]^{\rm T}$, and the regression matrix $\mathbf{B} \in \mathbb{R}^{K\times N_b}$ with

$$\mathbf{B} = \begin{bmatrix} B_1^{(P_o)}(|x_0|) & B_2^{(P_o)}(|x_0|) & \cdots & B_{N_b}^{(P_o)}(|x_0|) \\ B_1^{(P_o)}(|x_1|) & B_2^{(P_o)}(|x_1|) & \cdots & B_{N_b}^{(P_o)}(|x_1|) \\ \vdots & \vdots & \vdots & \vdots \\ B_1^{(P_o)}(|x_{N-1}|) & B_2^{(P_o)}(|x_{N-1}|) & \cdots & B_{N_b}^{(P_o)}(|x_{N-1}|) \end{bmatrix}. \tag{36}$$

Note that although $J_3(\boldsymbol{\omega})$ and $J_4(\boldsymbol{\theta})$ are not exactly equivalent to $J_2(\boldsymbol{\omega},\boldsymbol{\theta})$, they serves the same purpose of minimising the misalignment between the predicted HPA output $\widehat{w}_k$ by the two B-spline models to the desired output $\widetilde{w}_k$. Using $J_3(\boldsymbol{\omega})$ and $J_4(\boldsymbol{\theta})$ however can bring significant computational advantage, since we have the closed-form LS solutions of $\boldsymbol{\omega}$ and $\boldsymbol{\theta}$ given fixed $\boldsymbol{h}$. We adopt the following ALS algorithm, which is a coordinate gradient descent algorithm [20], [21], to estimate $\boldsymbol{h}$ as well as $\boldsymbol{\omega}$ and $\boldsymbol{\theta}$. The coordinate gradient descent approach transforms a difficult optimisation task into easier subtasks by fixing some variables in turn and solving the remaining variables. Unlike a generic coordinate gradient descent algorithm, in our case we have the closed-form solutions of $\boldsymbol{h}$ as well as $\boldsymbol{\omega}$ and $\boldsymbol{\theta}$ for the both subtasks.

Initialisation. Initialise $\widehat{w}_k = x_k$ in $\boldsymbol{P}$ of (29). Calculate $\boldsymbol{h}$ as the LS estimate given by $\widehat{\boldsymbol{h}}^{(0)} = \left(\boldsymbol{P}^{\rm H}\boldsymbol{P}\right)^{-1}\boldsymbol{P}^{\rm H}\boldsymbol{y}$. Then obtain $\widehat{\boldsymbol{h}}^{(0)}$ by normalising $h_i \leftarrow h_i/h_0$ for $0 \le i \le L_{\rm cir}$.

ALS estimation. For $1 \le \tau \le \tau_{\max}$, where $\tau_{\max}$ is the maximum number of iterations, perform:

a) Fix $\boldsymbol{h}$ to $\widehat{\boldsymbol{h}}^{(\tau-1)}$, and obtain $\widetilde{\boldsymbol{w}}$ using (16), (19) and (20). Then calculated $\widehat{\boldsymbol{\omega}}^{(\tau)}$ and $\widehat{\boldsymbol{\theta}}^{(\tau)}$ using (34) and (35).

b) For $\boldsymbol{P}$ of (29), compute $\widehat{w}_k$ according to (25) based on $\widehat{\boldsymbol{\omega}}^{(\tau)}$ and $\widehat{\boldsymbol{\theta}}^{(\tau)}$. Calculate $\widehat{\boldsymbol{h}}^{(\tau)}$ using (30). Then obtain $\widehat{\boldsymbol{h}}^{(\tau)}$ by normalising $h_i \leftarrow h_i/h_0$ for $0 \le i \le L_{\rm cir}$.

A few iterations, i.e. a very small $\tau_{\max}$, are sufficient for the above ALS estimation procedure to converge.

B. Inversion of the HPA's Nonlinear Amplitude Response

Given the CV Hammerstein channel's static nonlinearity $\Psi(\ )$, we wish to compute its inverse defined by $x_k = \Psi^{-1}(w_k)$. From (9), we have

$$|x_k| = A^{-1}(|w_k|), \tag{37}$$

$$\angle^{x_k} = \angle^{w_k} - \Upsilon(|x_k|). \tag{38}$$

Therefore, given the estimated HPA's amplitude response $\widehat{A}(\ )$ and phase response $\widehat{\Upsilon}(\ )$ specified by (23) and (24), we only need to find the inversion of $\widehat{A}(\ )$. We adopt the following B-spline neural network[1] to model $\widehat{A}^{-1}(\ )$

$$\left|\widehat{x}\right| = \widehat{A}^{-1}(|w|) = \sum_{l=1}^{N_b} B_l^{(P_o)}(|w|)\alpha_l. \tag{39}$$

In order to learn this inverse mapping or to estimate the parameter vector $\boldsymbol{\alpha} = \left[\alpha_1 \ \alpha_2 \cdots \alpha_{N_b}\right]^{\rm T}$, a training data set $\{|w_k|, |x_k|\}_{k=0}^{N-1}$ would be needed but w_k is unobservable and, therefore, is not available. Fortunately, as a byproduct of the Hammerstein channel identification presented in Section III-A, we already obtain an estimate for w_k as $\widehat{w}_k$ which is given in (25). Therefore, the pseudo training data $\left\{\left|\widehat{w}_k\right|, |x_k|\right\}_{k=0}^{N-1}$ can be utilised to estimate the inverse mapping (39). More specifically, by defining

$$\widehat{\mathbf{B}} = \begin{bmatrix} B_1^{(P_o)}(|\widehat{w}_0|) & B_2^{(P_o)}(|\widehat{w}_0|) & \cdots & B_{N_b}^{(P_o)}(|\widehat{w}_0|) \\ B_1^{(P_o)}(|\widehat{w}_1|) & B_2^{(P_o)}(|\widehat{w}_1|) & \cdots & B_{N_b}^{(P_o)}(|\widehat{w}_1|) \\ \vdots & \vdots & \vdots & \vdots \\ B_1^{(P_o)}(|\widehat{w}_{N-1}|) & B_2^{(P_o)}(|\widehat{w}_{N-1}|) & \cdots & B_{N_b}^{(P_o)}(|\widehat{w}_{N-1}|) \end{bmatrix}. \tag{40}$$

the LS solution of $\boldsymbol{\alpha}$ is readily given by $\widehat{\boldsymbol{\alpha}} = \left(\widehat{\mathbf{B}}^{\rm T}\widehat{\mathbf{B}}\right)^{-1}\widehat{\mathbf{B}}^{\rm T}\left|\boldsymbol{x}\right|$ in which $\left|\boldsymbol{x}\right| = \left[|x_0| \ |x_1| \cdots |x_{N-1}|\right]^{\rm T}$.

During the data detection, given the estimated CIR vector $\widehat{\boldsymbol{h}}$, the estimated nonlinear phase response $\widehat{\Upsilon}(\ )$ and the estimated inverse nonlinear amplitude response $\widehat{A}^{-1}(\ )$, the linear equalised TD signal $\widetilde{w}_k$ can be computed according to (16), (19) and (20). The estimate of the transmitted data x_k can then be given by $\widehat{x}_k = \left|\widehat{x}_k\right| \cdot e^{{\rm j}\angle^{\widehat{x}_k}}$ with $\left|\widehat{x}_k\right| = \widehat{A}^{-1}\left(\left|\widetilde{w}_k\right|\right)$ and $\angle^{\widehat{x}_k} = \angle^{\widetilde{w}_k} - \widehat{\Upsilon}\left(\left|\widehat{x}_k\right|\right)$.

[1] In order to avoid repetitions and for notational simplification, we keep the same B-spline notations of Section III-A and assume that the same number of basis functions and the polynomial order are used.

TABLE I

EMPIRICALLY DETERMINED KNOT SEQUENCES.

Knot sequence for $\|x\|$	0,	10^{-4},	10^{-3},	0.01,	0.03,	0.05,	1,	5,	10
Knot sequence for $\|\widehat{w}\|$	0,	10^{-4},	10^{-2},	0.2,	0.5,	2,	3,	4,	5

TABLE II

IDENTIFICATION RESULTS FOR THE CIR COEFFICIENT VECTOR $\boldsymbol{h}$ OF THE HAMMERSTEIN CHANNEL.

	True Parameters	Parameter estimate under			
		$E_{\rm b}/N_{\rm o} = 0$ dB OBO $= 5$ dB	$E_{\rm b}/N_{\rm o} = 10$ dB OBO $= 5$ dB	$E_{\rm b}/N_{\rm o} = 0$ dB OBO $= 2$ dB	$E_{\rm b}/N_{\rm o} = 10$ dB OBO $= 2$ dB
h_0	1	1	1	1	1
h_1	$-0.2145 - \text{j}0.1867$	$-0.2140 - \text{j}0.1870$	$-0.2143 - \text{j}0.1868$	$-0.2133 - \text{j}0.1873$	$-0.2140 - \text{j}0.1871$
h_2	$0.0399 + \text{j}0.3675$	$0.0408 + \text{j}0.3676$	$0.0402 + \text{j}0.3675$	$0.0410 + \text{j}0.3677$	$0.0402 + \text{j}0.3675$
h_3	$-0.0900 + \text{j}0.4053$	$-0.0897 + \text{j}0.4058$	$-0.0899 + \text{j}0.4055$	$-0.0893 + \text{j}0.4059$	$-0.0896 + \text{j}0.4054$
h_4	$-0.0893 + \text{j}0.1287$	$-0.0895 + \text{j}0.1286$	$-0.0894 + \text{j}0.1287$	$-0.0896 + \text{j}0.1286$	$-0.0895 + \text{j}0.1287$
h_5	$-0.1117 + \text{j}0.3035$	$-0.1118 + \text{j}0.3034$	$-0.1117 + \text{j}0.3034$	$-0.1115 + \text{j}0.3037$	$-0.1115 + \text{j}0.3038$
h_6	$-0.0766 - \text{j}0.0264$	$-0.0770 - \text{j}0.0266$	$-0.0768 - \text{j}0.0264$	$-0.0769 - \text{j}0.0266$	$-0.0765 - \text{j}0.0264$
h_7	$0.0623 - \text{j}0.0668$	$0.0628 - \text{j}0.0664$	$0.0625 - \text{j}0.0667$	$0.0628 - \text{j}0.0661$	$0.0623 - \text{j}0.0666$
h_8	$0.0282 + \text{j}0.0324$	$0.0272 + \text{j}0.0323$	$0.0279 + \text{j}0.0324$	$0.0264 + \text{j}0.0322$	$0.0275 + \text{j}0.0324$
h_9	$-0.0395 - \text{j}0.0291$	$-0.0395 - \text{j}0.0287$	$-0.0395 - \text{j}0.0290$	$-0.0398 - \text{j}0.084$	$-0.0397 - \text{j}0.0288$

IV. SIMULATION STUDY

We considered a Hammerstein SC-FDE System in which the HPA employed was described by (6) and (7) with the parameter set given in (8). The size of the transmitted data block was set to $N = 2048$ and 64-QAM was used. We assumed a quasi-static Rayleigh multipath channel with an exponentially decreasing power delay profile, where the average gain for the lth path was given by

$$\mathrm{E}\{|h_l|\} = e^{-\frac{l}{\eta}},\ 0 \le l \le L_{\rm cir}, \tag{41}$$

with η being the channel degradation factor. In the simulation study, we set $\eta = 3$ and $L_{\rm cir} = 9$. The CIR coefficients h_l for $0 \le l \le L_{\rm cir}$ remained constant during the communication session. We used a full data block with $N = 2048$ training samples in the joint estimation of the CIR coefficient vector $\boldsymbol{h}$ and the parameter vectors $\boldsymbol{\omega}$ and $\boldsymbol{\theta}$ of the two B-spline models for $\Psi(\ )$ as well as the estimation of the parameter vector $\boldsymbol{\alpha}$ of the inverting B-spline model for $A^{-1}(\ )$. The piecewise quadratic polynomial of $P_o = 2$ was chosen as the B-spline basis function, and the number of B-spline basis functions in all three B-spline neural networks was set to six. The empirically determined knot sequences for $|x_k|$ and $|\widehat{w}_k|$ are listed in Table. I. The system's signal-to-noise ratio (SNR) was defined as SNR $= E_{\rm b}/N_{\rm o}$, where $E_{\rm b}$ was the average power of the input signal x_k to the HPA and $N_{\rm o} = 2\sigma_e^2$ was the channel AWGN's power.

The identification experiments were conducted under the HPA operation conditions of OBO $= 5$ dB and OBO $= 2$ dB, respectively, as well as two given SNR conditions of SNR $=$ 0 dB and SNR $=$ 10 dB, respectively. The identification results of the linear subsystem in the Hammerstein channel under the four experimental conditions are summarised in Table II, while the modelling results of the HPA static nonlinearity $\Psi(\ )$ by the estimated $\widehat{\Psi}(\ )$ as represented by the two B-spline neural networks are illustrated in Fig. 1. It can be seen from Table II that the CIR estimates achieve high accuracy for all the four conditions. The results of Fig. 1 clearly demonstrate the capability of the proposed two RV B-spline neural networks to accurately model the HPA's nonlinear amplitude and phase response, respectively.

The combined response of the HPA's true nonlinearity and its estimated inversion obtained under the condition of OBO $=$ 2 dB and SNR $=$ 10 dB is depicted in Fig. 2. The result of Fig. 2 demonstrates the capability of the B-spline neural network to accurately model the inversion of the HPA's nonlinearity based only on the pseudo training data. The effectiveness of the proposed nonlinear SC-FDE scheme is illustrated in Fig. 3, where the nonlinear SC-FDE was constructed based on the estimated CIR $\widehat{\boldsymbol{h}}$, the estimated HPA's phase response $\widehat{\Upsilon}(\ )$ and the estimated inverse mapping for the HPA's amplitude response $\widehat{A}^{-1}(\ )$, obtained under the two simulation conditions. The achievable BER performance of the proposed nonlinear SC-FDE are plotted in Fig. 4 under three different operating conditions of the HPA, in comparison to the BER performance obtained by the standard linear SC-FDE. Clearly, the standard SC-FDE is incapable of compensating the nonlinear distortions of the Hammerstein channel and its attainable BER performance is very poor even under the HPA operating condition of OBO $=$ 5 dB, as can be seen from Fig. 4. By contrast, the proposed nonlinear SC-FDE constructed based on the estimated CIR and the inverse mapping of the HPA is able to compensate most of the nonlinear distortions and attains a much better BER performance.

V. CONCLUSIONS

A novel nonlinear SC-FDE scheme has been developed for the Hammerstein channel that includes the significant nonlin-

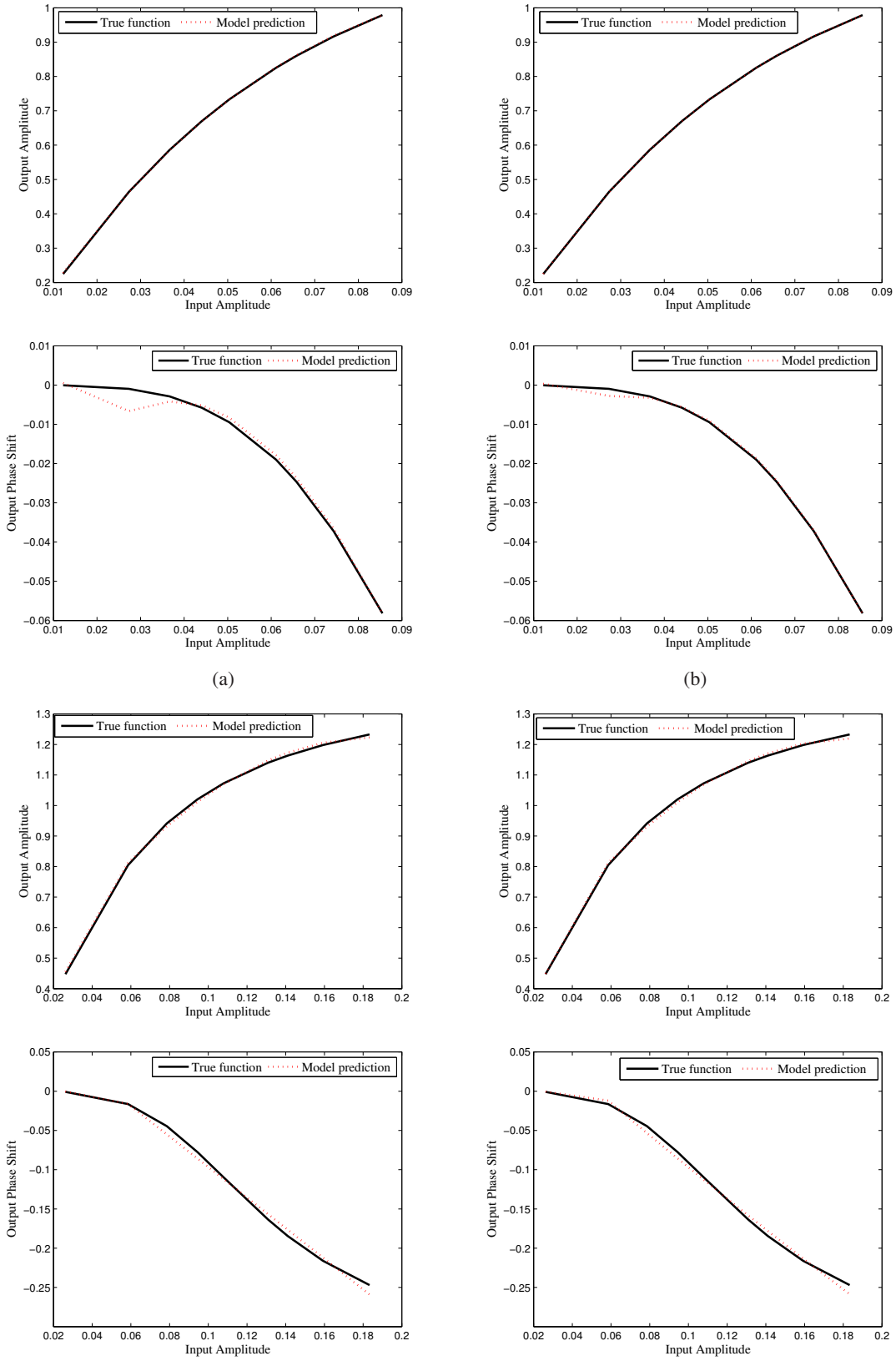

Fig. 1. Comparison of the HPA's static nonlinearity $\Psi(\ )$ and the estimated static nonlinearity $\widehat{\Psi}(\ )$ under: (a) OBO$=$ 5 dB, $E_{\rm b}/N_{\rm o} = 0$ dB; (b) OBO$=$ 5 dB, $E_{\rm b}/N_{\rm o} = 10$ dB; (c) OBO$=$ 2 dB, $E_{\rm b}/N_{\rm o} = 0$ dB; and (d) OBO$=$ 2 dB, $E_{\rm b}/N_{\rm o} = 10$ dB.

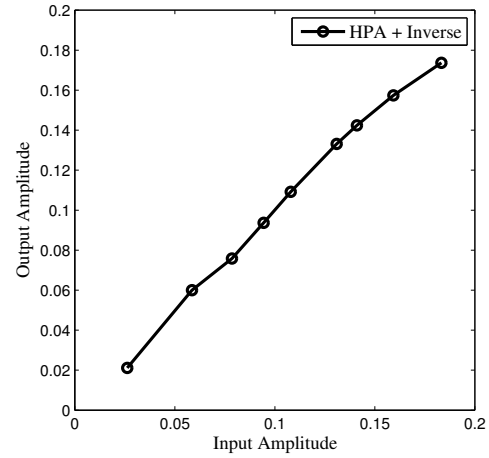

(a)

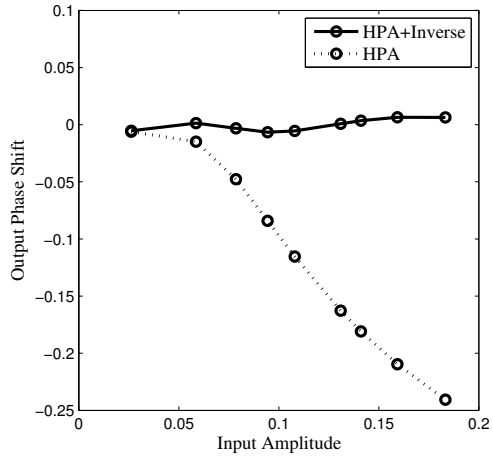

(b)

Fig. 2. Combined response of the true HPA and its estimated inversion obtained under OBO $= 2\,$dB and $E_{\rm b}/N_{\rm o} = 10\,$dB: (a) combined amplitude response, and (b) combined phase response.

ear distortions of the HPA at transmitter. We have proposed to utilise two RV B-spline neural networks for modelling the HPA's nonlinear amplitude and phase responses, respectively, and have derived an efficient ALS scheme to estimate the CIR coefficient vector as well as the parameter vectors of the two B-spline models that represent the HPA's nonlinearity. Moreover, an additional RV B-spline neural network has been utilised to model the inverse mapping of the HPA's amplitude response, and we have shown that the parameter vector of this inverting B-spline model can readily be obtained as the closed-form LS solution based on the pseudo training data obtained as a natural byproduct of the Hammerstein channel identification. Simulation results have demonstrated that our proposed identification procedure is capable of accurately estimating the Hammerstein channel as well as the inverse mapping of the channel's static nonlinearity. The results obtained have also confirmed the effectiveness of the proposed nonlinear SC-FDE scheme constructed based on the estimated CIR and inverse B-spline mapping.

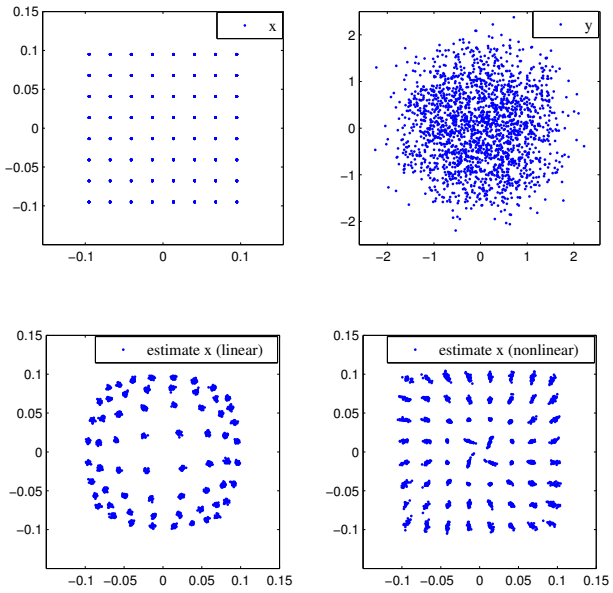

(a)

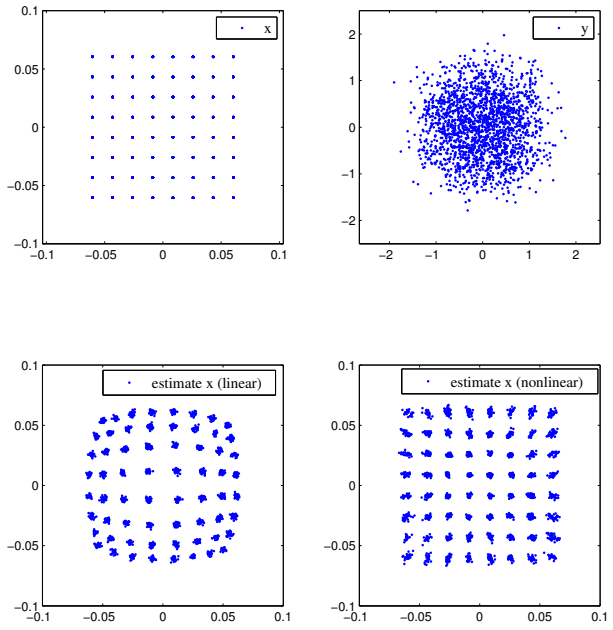

(b)

Fig. 3. Effectiveness of the proposed nonlinear SC-FDE scheme based on the estimated CIR $\widehat{\boldsymbol{h}}$ and the estimated HPA's CV static nonlinearity as well as the estimated inverse mapping for the HPA's amplitude response under: (a) OBO $= 3\,$dB and $E_{\rm b}/N_{\rm o} = 10\,$dB; and (b) OBO $= 5\,$dB and $E_{\rm b}/N_{\rm o} = 4\,$dB. The top two plots in sub-figures (a) and (b) depict one transmitted QAM symbol block $\boldsymbol{x}$ and its received signal block $\boldsymbol{y}$, while the bottom two plots show the corresponding estimated $\widehat{\boldsymbol{x}}$ obtained by the linear and nonlinear SC-FDEs, respectively.

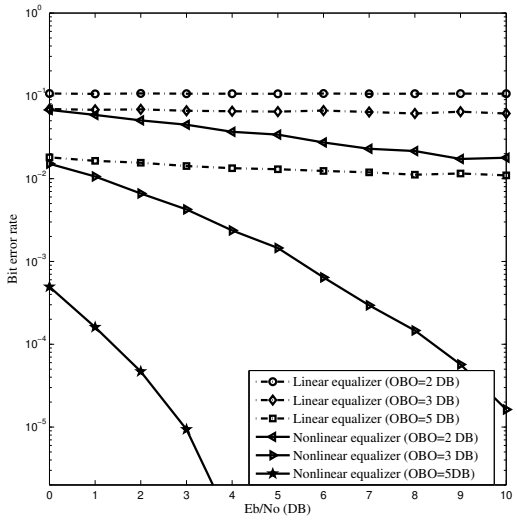

Fig. 4. The bit error rate performance comparison of the proposed nonlinear SC-FDE with the standard linear SC-FDE.

APPENDIX

A. De Boor Recursion

Univariate RV B-spline basis functions are parametrized by the order $(P_0 - 1)$ of a piecewise polynomial and a knot sequence which is a set of values defined on the real line that break it up into a number of intervals. Let the number of basis functions be N_b. The knot sequence is specified by the $(N_b + P_0 + 1)$ knot values $\{R_0, R_1, \cdots, R_{N_b+P_0}\}$ with

$$R_0 < R_1 < \cdots < R_{P_0-2} < R_{P_0-1} = R_{\min} < R_{P_0} < \cdots < R_{N_b} < R_{N_b+1} = R_{\max} < R_{N_b+2} < \cdots < R_{N_b+P_0}. \quad (42)$$

At each end, there are $P_o - 1$ external knots that are outside the input region and one boundary knot. As a result, the number of internal knots is $N_b + 1 - P_0$. Given the set of predetermined knots (42), the set of N_b B-spline basis functions can be formed by using the De Boor recursion [22], yielding for $1 \le l \le N_b + P_0$,

$$B_l^{(0)}(r) = \begin{cases} 1, & \text{if } R_{l-1} \le r < R_l, \\ 0, & \text{otherwise,} \end{cases} \quad (43)$$

as well as for $l = 1, \cdots, N_b + P_0 - p$ and $p = 1, \cdots, P_0$,

$$B_l^{(p)}(r) = \frac{r - U_{l-1}}{U_{p+l-1} - U_{l-1}} B_l^{(p-1)}(r) + \frac{U_{p+l} - r}{U_{p+l} - U_l} B_{l+1}^{(p-1)}(r). \quad (44)$$

Note that, due to the piecewise nature of B-spline functions, there are only $P_0 + 1$ basis functions with nonzero functional values at any point r. Hence, the complexity of the De Boor algorithm is determined by the polynomial order P_0, rather than the number of knots, and this is in the order of $\mathcal{O}\big(P_0^2\big)$.

REFERENCES

[1] J. A. C. Bingham, "Multicarrier modulation for data transmission: an idea whose time has come," *IEEE Communications Magazine*, vol. 28, no. 5, pp. 5–14, May 1990.

[2] L. Hanzo, M. Münster, B. J. Choi, and T. Keller, *OFDM and MC-CDMA for Broadband Multi-User Communications, WLANs, and Broadcasting*. Chichester, UK: Wiley, 2003.

[3] A. A. M. Saleh, "Frequency-independent and frequency-dependent nonlinear models of TWT amplifiers," *IEEE Trans. Communications*, vol. COM-29, no. 11, pp.1715–1720, Nov. 1981.

[4] M. Honkanen and S.-G. Häggman, "New aspects on nonlinear power amplifier modeling in radio communication system simulations," in *Proc. PIMRC'97* (Helsinki, Finland), Sept. 1-4, 1997, pp. 844–848.

[5] C. J. Clark, G. Chrisikos, M. S. Muha, A. A. Moulthrop, and C. P. Silva, "Time-domain envelope measurement technique with application to wideband power amplifier modeling," *IEEE Trans. Microwave Theory and Techniques*, vol. 46, no. 12, pp. 2531–2540, Dec. 1998.

[6] C.-S. Choi, *et al.*,"RF impairment models 60 GHz band SYS/PHY simulation," Document IEEE 802.15-06-0477-01-003c, Nov. 2006. https://mentor.ieee.org/802.15/dcn/06/15-06-0477-01-003c-rf-impairment-models-60ghz-band-sysphy-simulation.pdf

[7] V. Erceg, *et al.*, "60 GHz impairments modeling," Document IEEE 802.11-09/1213r1, Nov. 2009.

[8] D. Falconer, S. L. Ariyavisitakul, A. Benyamin-Seeyar, and B. Eidson, "Frequency domain equalization for single carrier broadband wireless systems," *IEEE Communications Magazine*, vol. 40, no. 4, pp. 58–66, April 2002.

[9] F. Pancaldi, G. M. Vitetta, R. Kalbasi, N. Al-Dhahir, M. Uysal, and H. Mheidat, "Single-carrier frequency domain equalization," *IEEE Signal Processing Magazine*, vol. 25, no. 5, pp. 37–56, Sept. 2008.

[10] E. Seidel, "Progress on 'LTE Advanced' - the new 4G standard," Nomor Research GmbH: White Paper on LTE Advanced, 2008.

[11] L. Hanzo, S. X. Ng, T. Keller, and W. Webb, *Quadrature Amplitude Modulation: From Basics to Adaptive Trellis-Coded, Turbo-Equalised and Space-Time Coded OFDM, CDMA and MC-CDMA Systems*. Chichester, UK: John Wiley, 2004.

[12] L. Ding, G. T. Zhou, D. R. Morgan, Z. Ma, J. S. Kenney, J. Kim, and C. R. Giardina, "A robust digital baseband predistorter constructed using memory polynomials," *IEEE Trans. Communications*, vol. 52, no. 1, pp. 159–165, Jan. 2004.

[13] D. Zhou and V. E. DeBrunner, "Novel adaptive nonlinear predistorters based on the direct learning algorithm," *IEEE Trans. Signal Processing*, vol. 55, no. 1, pp. 120–133, Jan. 2007.

[14] M.-C. Chiu, C.-H. Zeng, and M.-C. Liu, "Predistorter based on frequency domain estimation for compensation of nonlinear distortion in OFDM systems," *IEEE Trans. Vehicular Technology*, vol. 57, no. 2, pp. 882–892, March 2008.

[15] S. Choi, E.-R. Jeong, and Y. H. Lee, "Adaptive predistortion with direct learning based on piecewise linear approximation of amplifier nonlinearity," *IEEE J. Selected Topics in Signal Processing*, vol. 3, no. 3, pp. 397–404, June 2009.

[16] V. P. G. Jiménez, Y. Jabrane, A. G. Armada, and B. Ait Es Said, "High power amplifier pre-distorter based on neural-fuzzy systems for OFDM signals," *IEEE Trans. Broadcasting*, vol.57, no. 1, pp. 149–158, March 2011.

[17] S. Chen, "An efficient predistorter design for compensating nonlinear memory high power amplifier," *IEEE Trans. Broadcasting*, vol. 57, no. 4, pp. 856–865, Dec. 2011.

[18] S. Chen, X. Hong, Y. Gong, and C. J. Harris, "Digital predistorter design using B-spline neural network and inverse of De Boor algorithm," *IEEE Trans. Circuits and Systems I*, vol. 60, no. 6, pp. 1584–1594, June 2013.

[19] X. Hong, S. Chen, and C. J. Harris, "Complex-valued B-spline neural networks for modeling and inverse of Wiener systems," Chapter 9 in: A. Hirose, ed. *Complex-Valued Neural Networks: Advances and Applications*. Hoboken, NJ: IEEE and Wiley, 2013, pp. 209–233.

[20] R. J. Hathaway and J. C. Bezdek, "Grouped coordinate minimization using Newton's method for inexact minimization in one vector coordinate," *J. Optimization Theory and Applications*, vol. 71, no. 3, pp. 503–516, Dec. 1991.

[21] Z. Q. Luo and P. Tseng, "On the convergence of the coordinate descent method for convex differentiable minimization," *J. Optimization Theory and Applications*, vol. 72, no. 1, pp. 7–35, Jan. 1991.

[22] C. De Boor, *A Practical Guide to Splines*. New York: Spring Verlag, 1978.